Supporting Information for "Morphodynamic equilibria in short tidal basins using a 2DH exploratory model"

Thomas Boelens[1]*, Tian Qi[1]*, Henk Schuttelaars[2], Tom De Mulder[1]

[1]Hydraulics Laboratory, Department of Civil Engineering, Ghent University, Belgium
[2]Delft Institute of Applied Mathematics, Delft University of Technology, The Netherlands

Appendix A Dimensionless equations

The governing equations are made dimensionless by introducing characteristic scales for the physical variables (dimensionless variables are denoted with asterisk):

$$(x, y) = L(x^*, y^*); \quad (u, v) = U(u^*, v^*); \quad \zeta = \overline{A_{M_2}}\zeta^*; \quad C = \frac{\alpha U^2 \kappa_v}{{w_s}^2} C^*; \quad t = \sigma^{-1} t^*;$$
$$(z, h) = \overline{H}(z^*, h^*); \quad (\mu, \lambda) = \sigma L^2 (\mu^*, \lambda^*); \quad r = (\sigma \overline{H}) r^*; \quad \beta = \beta^*; \quad f = \sigma f^*. \tag{A.1}$$

The characteristic scales include the length L of the basin, the tidally and width-averaged water depth at the open boundary $\overline{H}$, the width-averaged water level amplitude at the open boundary $\overline{A_{M_2}}$ and the angular frequency σ of the semidiurnal tide. The velocity scale follows from the continuity equation (2.1a) in the main text and reads $U = \sigma \overline{A_{M_2}} L/\overline{H}$, while the friction scale and Coriolis scale follow from the momentum equation. Assuming an approximate balance between erosion and deposition, the depth-integrated suspended sediment concentration is scaled with the ratio of the typical scale of the erosion term (αU^2) and the proportionality constant of the deposition term (${w_s}^2/\kappa_v$).

The dimensionless equations for the water motion read

$$\zeta^*_{t^*} + \vec{\nabla}^* \cdot [(1 - h^*)\vec{u}^*] = 0, \tag{A.2a}$$
$$(1 - h^* + h_0^*) \left[\vec{u}^*_{t^*} + \eta^{*-2} \vec{\nabla}^* \zeta^* + \vec{f}_c^* \right] + r^* \vec{u}^* = \vec{0}, \tag{A.2b}$$

where the momentum equation has been multiplied with $(1 - h^* + h_0^*)$, i.e. the local tidally averaged water depth, adjusted with $h_0^* = h_0/\overline{H}$. As mentioned before, the parameter h_0^* is introduced to ensure that the bottom friction term remains bounded if the water depth goes to zero. The parameter $\eta^* = (\sigma L)/\sqrt{g\overline{H}}$ in (A.2b) is, apart from a factor 2π, the ratio of the estuary length, L, and the frictionless tidal wavelength in a straight channel without tidal flats, $L_g = 2\pi\sqrt{g\overline{H}}/\sigma$. The vector $\vec{f}_c^*$ is defined as $\vec{f}_c^{\,*} = (-f^* v^*, f^* u^*)^{\mathrm{T}}$, which can also be formulated as the dot product $\vec{f}_c^{\,*} = \mathbf{F} \cdot \vec{u}^*$ of the velocity vector $\vec{u}^* = (u^*, v^*)^{\mathrm{T}}$ and the matrix $\mathbf{F} = \begin{bmatrix} 0 & -f \\ f & 0 \end{bmatrix}$.

The dimensionless concentration equation becomes

*These authors contributed equally to this work.

Corresponding author: Tian Qi, Tian.Qi@UGent.be

$$a^* \left[C^*_{t^*} - \vec{\nabla}^* \cdot \left(\mu^* \vec{\nabla}^* C^* + \mu^* \Lambda^* \beta^* C^* \vec{\nabla}^* h^* \right) \right] = |\vec{u}^*|^2 - \beta^* C^*. \tag{A.3}$$

Here $a^* = \frac{\sigma \kappa_v}{{w_s}^2}$ is the ratio of the time scale of the deposition process over the tidal time scale and $\Lambda^* = \frac{w_s H}{\kappa_v}$ is the sediment Peclet number. The dimensionless deposition parameter β^* can be written in terms of dimensionless variables as

$$\beta^* = \left[1 - e^{-\Lambda^* (1 - h^* + h_0^*)} \right]^{-1}. \tag{A.4}$$

Finally, the scaled bed evolution equation is given by

$$\begin{aligned} h^*_{\tau^*} &= - \left\langle |\vec{u}^*|^2 - \beta^* C^* \right\rangle + \delta^{-1} \lambda^* \nabla^{*2} h^* \\ &= -\vec{\nabla}^* \cdot \Bigg\langle \underbrace{- \delta^{-1} \lambda^* \vec{\nabla}^* h^*}_{\vec{q}^*_{\mathrm{bl}}} \underbrace{- a^* \mu^* \vec{\nabla}^* C^*}_{\vec{q}^*_{\mathrm{diff}}} \underbrace{- a^* \mu^* \Lambda^* \beta^* C^* \vec{\nabla}^* h^*}_{\vec{q}^*_{\mathrm{topo}}} \Bigg\rangle, \\ &= -\vec{\nabla}^* \cdot \langle \vec{q}^* \rangle \end{aligned} \tag{A.5}$$

with $\tau^* = \delta t^*$, where $\delta = \alpha U^2 / [\sigma \overline{H} \rho_s (1 - p)]$ is the ratio of the tidal period and the slow morphodynamic timescale.

The dimensionless sediment transport $\vec{q}^*$ consists of bedslope effects of bedload transport, as well as diffusive and topographically induced diffusive contributions to the suspended sediment transport:

$$\vec{q}^* = \vec{q}^*_{\mathrm{bl}} + \vec{q}^*_{\mathrm{diff}} + \vec{q}^*_{\mathrm{topo}}. \tag{A.6}$$

The dimensionless boundary conditions read

$$\zeta^* = A^*_{M_2} \cos(t^* - \theta_{M_2}) \qquad \text{for } (x^*, y^*) \in \Gamma_o, \tag{A.7a}$$

$$\left\langle |\vec{u}^*|^2 - \beta^* C^* \right\rangle = 0 \qquad \text{for } (x^*, y^*) \in \Gamma_o, \tag{A.7b}$$

$$\overline{h^*} = 0 \qquad \text{at } \Gamma_o, \tag{A.7c}$$

$$(1 - h^*)\, \vec{u}^* \cdot \vec{n} = 0 \qquad \text{for } (x^*, y^*) \in \Gamma_c, \tag{A.7d}$$

$$\left\langle \delta^{-1} \lambda^* \vec{\nabla}^* h^* + a^* \mu^* (\vec{\nabla}^* C^* + \Lambda^* \beta^* C^* \vec{\nabla}^* h^*) \right\rangle \cdot \vec{n} = \langle \vec{q}^* \rangle \cdot \vec{n} = 0 \qquad \text{for } (x^*, y^*) \in \Gamma_c, \tag{A.7e}$$

where $A^*_{M_2} = A_{M_2} / \overline{A_{M_2}}$. Note that A_{M_2} and θ_{M_2} depend on the x^* and y^* coordinates at the open seaward boundary Γ_o.

Appendix B Relative importance of advective processes

B.1 Depth-averaged shallow water equations

If the nonlinear terms, including the advective ones, were taken into account in the continuity and momentum equations, the dimensionless equations (A.2a) and (A.2b) need to be modified as follows:

$$\zeta^*_{t^*} + \vec{\nabla}^* \cdot [(1 - h^* + \epsilon\zeta^*)\vec{u}^*] = 0, \tag{B.1a}$$

$$(1 - h^* + \epsilon\zeta^* + h^*_o)\left[\vec{u}^*_{t^*} + \epsilon\,(\vec{u}^* \cdot \vec{\nabla}^*)\,\vec{u}^* + {\eta^*}^{-2}\vec{\nabla}^*\zeta^* + \vec{f}^*_c\right] + r^*\vec{u}^* = 0, \tag{B.1b}$$

in which the nonlinear terms are found to be scaled with the small parameter $\epsilon = \frac{U}{\sigma L} = \frac{\overline{A_{M_2}}}{\overline{H}}$ (~ 0.1, see Table 1 in the main text). This shows that the nonlinear terms are an order of magnitude smaller than the terms of $O(1)$.

B.2 Depth-integrated concentration equation

If advective transport of suspended sediment were taken into account, the dimensionless equation (A.3) for the depth-integrated concentration needs to be modified as follows:

$$a^*\left[C^*_{t^*} + \vec{\nabla}^* \cdot \left(\epsilon\vec{u}^*C^* - \mu^*\vec{\nabla}^*C^* - \mu^*\Lambda^*\beta^*C^*\vec{\nabla}^*h^*\right)\right] = |\vec{u}^*|^2 - \beta^*C^*, \tag{B.2}$$

in which the advective transport is scaled with the small parameter ϵ, while the diffusive transport is scaled with the parameter $\mu^* = \frac{\mu}{\sigma L^2}$ (~ 0.003, see Table 1 in main text). Hence, advective transport is (~ 30 times) more important than diffusive transport in the time-dependent equation for the instantaneous depth-integrated concentration.

B.3 Tidally averaged total sediment transport

If advective transport of suspended sediment concentration were taken into account, the dimensionless total sediment transport $\vec{q}^*$ in eq. (A.6) gets an extra advective contribution:

$$\vec{q}^* = \vec{q}^*_{\text{bl}} + \vec{q}^*_{\text{diff}} + \vec{q}^*_{\text{topo}} + \vec{q}^*_{\text{adv}}\,, \tag{B.3}$$

and the dimensionless bed evolution eq. (A.5) would read as follows:

$$\begin{aligned} h^*_{\tau^*} &= -\vec{\nabla}^* \cdot \Bigg\langle \underbrace{-\delta^{-1}\lambda^*\vec{\nabla}^*h^*}_{\vec{q}^*_{\text{bl}}} \underbrace{-a^*\mu^*\vec{\nabla}^*C^*}_{\vec{q}^*_{\text{diff}}} \underbrace{-a^*\mu^*\Lambda^*\beta^*C^*\vec{\nabla}^*h^*}_{\vec{q}^*_{\text{topo}}} \underbrace{+a^*\epsilon\vec{u}^*C^*}_{\vec{q}^*_{\text{adv}}} \Bigg\rangle, \\ &= -\vec{\nabla}^* \cdot \langle\vec{q}^*\rangle \end{aligned} \tag{B.4}$$

For short tidal inlet systems considered in this paper, the length is much smaller than the frictionless tidal wavelength. In this case, the parameter $\eta^* = (\sigma L)/\sqrt{g\overline{H}}$ (~ 0.2, see Table 1 in main text) is much smaller than one and the momentum equation (eq. A.2b) reduces in good approximation to $\vec{\nabla}^*\zeta^* = \vec{0}$. This implies that at every moment in time, the free sea surface in the basin is spatially uniform and equal to the surface elevation imposed at the open boundary

(eq. A.7a), see De Vriend and Ribberink (1996); Schuttelaars and de Swart (1996); Ter Brake and Schuttelaars (2011). The basin is then said to be in a "pumping mode".

Similar to the scaling analysis presented by Schuttelaars and de Swart (1996); de Swart and Blaas (1998); Ter Brake and Schuttelaars (2010, 2011), it is further explained in this Appendix how the various contributions to the (tidally-averaged) total sediment transport scale.

To this end, approximate solutions to the (dimensionless) equations governing the water motion and sediment transport in pumping mode are obtained, by expanding the velocity and depth-integrated concentration, as well as the deposition parameter, in the small parameter ϵ:

$$\vec{u}^* = \vec{u}_0^* + \epsilon \vec{u}_1^* + \cdots, \tag{B.5a}$$

$$C^* = C_0^* + \epsilon C_1^* + \cdots, \tag{B.5b}$$

$$\beta^* = \beta_0^* + \epsilon \beta_1^* + \cdots. \tag{B.5c}$$

By inserting the expansions up to the first-order terms in the governing equations, separate expressions can be derived which govern the zeroth-order unknowns ($\vec{u}_0^*$ and C_0^*) and the first-order unknowns ($\vec{u}_1^*$ and C_1^*).

Using the pumping mode assumption, the zeroth-order velocity follows from the continuity equation (A.2a) and the leading-order vorticity equation (see Ter Brake and Schuttelaars (2011)). Using the boundary conditions eqs. (A.7a) and (A.7d), it follows that the leading-order water motion only consists of an M_2 tidal constituent.

The zeroth-order depth-integrated sediment concentration follows from:

$$a^* \left[\left(C_0^*\right)_{t^*} - \vec{\nabla}^* \cdot \left(\mu^* \vec{\nabla}^* C_0^* + \mu^* \Lambda^* \beta_0^* C_0^* \vec{\nabla}^* h^* \right) \right] = |\vec{u}_0^*|^2 - \beta_0^* C_0^*. \tag{B.6}$$

Since the leading-order solution C_0^* is only forced by $|\vec{u}_0^*|^2$, it follows that it consists of a residual contribution and a contribution with a period twice that of the M_2 tide. As a consequence, the tidally averaged advective transport $\left\langle \vec{u}_0^* C_0^* \right\rangle = 0$.

Similarly, expressions can be derived for the first-order velocity $\vec{u}_1^*$ and the depth-integrated concentration C_1^*. Careful analysis shows that the first-order velocity consists of a residual and an M_4 component, while the first-order depth-integrated concentration has an M_2 component.

When inserting the expansions of $\vec{u}^*$, C^*, and β^* up to first order in the small parameter ϵ into the bed evolution equation, the leading-order terms of the various contributions to the tidally-averaged total sediment transport read:

$$\left\langle \vec{q}^*_{\mathrm{bl}} \right\rangle = -\delta^{-1}\lambda^*\vec{\nabla}^* h^*\,, \tag{B.7a}$$

$$\left\langle \vec{q}^*_{\mathrm{diff}} \right\rangle = -a^*\mu^*\vec{\nabla}^* \left\langle C^*_0 \right\rangle\,, \tag{B.7b}$$

$$\left\langle \vec{q}^*_{\mathrm{topo}} \right\rangle = -a^*\mu^*\Lambda^*\beta^*_0 \left\langle C^*_0 \right\rangle \vec{\nabla}^* h^*, \tag{B.7c}$$

$$\begin{aligned}\left\langle \vec{q}^*_{\mathrm{adv}} \right\rangle &= a^*\epsilon \left\langle \vec{u}^* C^* \right\rangle = a^*\epsilon \left[\underbrace{\left\langle \vec{u}^*_0 C^*_0 \right\rangle}_{=0} + \epsilon \left(\left\langle \vec{u}^*_0 C^*_1 \right\rangle + \left\langle \vec{u}^*_1 C^*_0 \right\rangle \right) \right], \\ &= a^*\epsilon^2 \left(\left\langle \vec{u}^*_0 C^*_1 \right\rangle + \left\langle \vec{u}^*_1 C^*_0 \right\rangle \right)\,. \end{aligned} \tag{B.7d}$$

For a short basin (pumping mode), the tidal averages of the correlations $\vec{u}^*_0 C^*_1$ and $\vec{u}^*_1 C^*_0$ scale with a^* (since the temporal parts of the concentrations contain a^*), resulting in a tidally-averaged advective transport that is proportional to $a^{*2}\epsilon^2$ (Schuttelaars & de Swart, 1996; Ter Brake & Schuttelaars, 2010).

From the foregoing expressions, the order of magnitude of the different contributions to the total sediment transport $\langle \vec{q}^* \rangle$ can be estimated, using the typical values for the tidal inlet systems we consider (see Table 1 in the main text):

- $\left\langle \vec{q}^*_{\mathrm{bl}} \right\rangle$ scales as $\delta^{-1}\lambda^* = \frac{\sigma \overline{H}\rho(1-p)}{\alpha U^2}\frac{\lambda}{\sigma L^2} = \frac{\overline{H}^3\rho(1-p)\lambda}{\alpha \overline{A_{M_2}}^2 \sigma^2 L^4} \sim 1\times 10^{-6}$,
- $\left\langle \vec{q}^*_{\mathrm{diff}} \right\rangle$ scales as $a^*\mu^* = \frac{\sigma\kappa_v}{w_s^2}\frac{\mu}{\sigma L^2} = \frac{\kappa_v \mu}{w_s^2 L^2} \sim 2\times 10^{-4}$,
- Since $\Lambda^* = \frac{w_s \overline{H}}{\kappa_v} \sim 1.5$ and $h^*_o \sim 0.4$, it follows that β^*_0 is in the range 1.1 to 2.2 for h^* varying between 0 and 1. Consequently, $\left\langle \vec{q}^*_{\mathrm{topo}} \right\rangle$ scales as $a^*\mu^*\Lambda^*\beta^*_0 \sim (3\,\text{to}\,7)\times 10^{-4}$,
- $\left\langle \vec{q}^*_{\mathrm{adv}} \right\rangle$ scales as $\left(\frac{\sigma\kappa_v}{w_s^2}\frac{\overline{A_{M_2}}}{\overline{H}}\right)^2 \sim 4\times 10^{-5}$.

Despite the fact that *instantaneous* advective transport dominates diffusive transport in the depth-integrated concentration equation (section B.2), the foregoing scaling analysis of the *tidally averaged* total sediment transport $\langle \vec{q}^* \rangle$ shows that the *tidally averaged* advective contribution $\left\langle \vec{q}^*_{\mathrm{adv}} \right\rangle$ is an order of magnitude smaller than the *tidally averaged* diffusive contributions, confirming that *tidally averaged* diffusive transport is dominant for short tidal inlet systems.

This conclusion is also supported by results presented in van Leeuwen and de Swart (2001); Chapter 3 of van Leeuwen (2002); van Leeuwen and de Swart (2004). In these papers, it is shown that for the parameter values used in our paper, the tidally averaged sediment transport is dominated by diffusive transport, with advective transport resulting in a correction on the diffusive transport, see Figure 3.10 in van Leeuwen (2002), where it is shown that the divergence of the tidally advective transport is approximately a factor 10 smaller than that of the diffusive transport. A similar figure is found in van Leeuwen and de Swart (2001). In their 2004 paper, they show that the growth rates of the bed patterns, obtained with the idealised and the numerical (Delft3D) model show a very good correspondence (see Figs. 8 and 9 in van Leeuwen and de Swart (2004)), implying that the dynamics is well-captured by the idealised model and hence that also in the Delft3D model the bottom changes are dominated by convergences and divergences of tidally averaged diffusive transports.

B.4 Conclusions

In this Appendix, the relative importance of advective processes has been investigated for the short tidal inlet systems considered in this work.

Section B.1 demonstrated that the nonlinear terms, including the advective ones, can as a first approximation be neglected from the depth-averaged shallow water equations. Therefore, no nonlinear terms are accounted for in eq. (2.1a) and (2.1b) of the main text.

Section B.3 has shown that the advective contribution to the tidally averaged suspended sediment transport is an order of magnitude smaller than the diffusive contributions. Since the main focus of this paper is on the identification of morphodynamic equilibria, and the latter only depend on the tidally averaged sediment transport, the advective transport term is not included in the depth-integrated suspended sediment concentration equation (2.3) in the main text, despite the fact that section B.2 has shown advective transport to dominate diffusive transport in the time-dependent concentration equation. Note that the tidally averaged depth-integrated concentrations shown in (Figures 5 and 10 of) the main text follow from an approximate balance between erosion and deposition, which implies that advection (neglected in eq. (2.3)) and diffusion (included in eq. (2.3)) only modify it.

Since the advective contribution to the tidally averaged suspended sediment transport is discarded, there is no need for $O(\epsilon^1)$ velocities, $\vec{u}_1^*$, yielding an additional reason for not including the advective acceleration term in the momentum equation (2.1b).

Appendix C Linearised dimensionless equations in variational form

The nonlinear system of equations is solved numerically using a fixed-point method (Newton's method), formulated at the partial differential equation (PDE) level. The asterisk notation has been omitted to simplify the notation. Given an initial guess for the solution of each of the variables χ^0 we seek a small perturbation δ^χ, such that $\chi = \chi^0 + \delta^\chi$ fulfills the nonlinear system of PDEs. Note that for the bed level h^0 is the intitial guess, while h_0 is a parameter to assure the friction term remains finite. Using equations (2.12) and (2.13) in the main text, the system of equations then becomes

$$\delta^{\zeta_{s1}} + \vec{\nabla}\cdot\left[(1-h^0)\,\delta^{\vec{u}_{c1}} - \delta^h\,\vec{u}^0_{c1}\right] = -\zeta^0_{s1} - \vec{\nabla}\cdot\left[(1-h^0)\,\vec{u}^0_{c1}\right], \tag{C.1a}$$

$$-\delta^{\zeta_{c1}} + \vec{\nabla}\cdot\left[(1-h^0)\,\delta^{\vec{u}_{s1}} - \delta^h\,\vec{u}^0_{s1}\right] = \zeta^0_{c1} - \vec{\nabla}\cdot\left[(1-h^0)\,\vec{u}^0_{s1}\right], \tag{C.1b}$$

$$\begin{aligned}(1-h^0+h_0)\left(\delta^{\vec{u}_{s1}} + \eta^{-2}\vec{\nabla}\delta^{\zeta_{c1}} + \mathbf{F}\cdot\delta^{\vec{u}_{c1}}\right) - \delta^h\left(\vec{u}^0_{s1} + \eta^{-2}\vec{\nabla}\zeta^0_{c1} + \mathbf{F}\cdot\vec{u}^0_{c1}\right)\\ + r\delta^{\vec{u}_{c1}} = -(1-h^0+h_0)\left(\vec{u}^0_{s1} + \eta^{-2}\vec{\nabla}\zeta^0_{c1} + \mathbf{F}\cdot\vec{u}^0_{c1}\right) - r\vec{u}^0_{c1},\end{aligned} \tag{C.1c}$$

$$\begin{aligned}(1-h^0+h_0)\left(-\delta^{\vec{u}_{c1}} + \eta^{-2}\vec{\nabla}\delta^{\zeta_{s1}} + \mathbf{F}\cdot\delta^{\vec{u}_{s1}}\right) - \delta^h\left(-\vec{u}^0_{c1} + \eta^{-2}\vec{\nabla}\zeta^0_{s1} + \mathbf{F}\cdot\vec{u}^0_{s1}\right)\\ + r\delta^{\vec{u}_{s1}} = -(1-h^0+h_0)\left(-\vec{u}^0_{c1} + \eta^{-2}\vec{\nabla}\zeta^0_{s1} + \mathbf{F}\cdot\vec{u}^0_{s1}\right) - r\vec{u}^0_{s1},\end{aligned} \tag{C.1d}$$

$$\begin{aligned}&-a\mu\vec{\nabla}\cdot\left[\vec{\nabla}\delta^{\langle C\rangle} + \Lambda\left(\delta^\beta\left\langle C^0\right\rangle\vec{\nabla}h^0 + \beta^0\delta^{\langle C\rangle}\vec{\nabla}h^0 + \beta^0\left\langle C^0\right\rangle\vec{\nabla}\delta^h\right)\right]\\ &\quad - \vec{u}^0_{c1}\cdot\delta^{\vec{u}_{c1}} - \vec{u}^0_{s1}\cdot\delta^{\vec{u}_{s1}} + \delta^\beta\left\langle C^0\right\rangle + \beta^0\delta^{\langle C\rangle}\\ &\quad = a\mu\vec{\nabla}\cdot\left(\vec{\nabla}\left\langle C^0\right\rangle + \Lambda\beta^0\left\langle C^0\right\rangle\vec{\nabla}h^0\right) + \frac{1}{2}\left(|\vec{u}^0_{c1}|^2 + |\vec{u}^0_{s1}|^2\right) - \beta^0\left\langle C^0\right\rangle,\end{aligned} \tag{C.1e}$$

$$\begin{aligned}&-a\mu\vec{\nabla}\cdot\left[\vec{\nabla}\delta^{\langle C\rangle} + \Lambda\left(\delta^\beta\left\langle C^0\right\rangle\vec{\nabla}h^0 + \beta^0\delta^{\langle C\rangle}\vec{\nabla}h^0 + \beta^0\left\langle C^0\right\rangle\vec{\nabla}\delta^h\right)\right] - \lambda\nabla^2\delta^h\\ &\quad = a\mu\vec{\nabla}\cdot\left(\vec{\nabla}\left\langle C^0\right\rangle + \Lambda\beta^0\left\langle C^0\right\rangle\vec{\nabla}h^0\right) + \lambda\nabla^2 h^0,\end{aligned} \tag{C.1f}$$

with

$$\beta^0 = \frac{1}{1-e^{-\Lambda(1-h^0+h_0)}}, \qquad \delta^\beta = \delta^h\frac{\Lambda e^{-\Lambda(1-h^0+h_0)}}{\left(1-e^{-\Lambda(1-h^0+h_0)}\right)^2}. \tag{C.2}$$

The dimensionless boundary conditions then become

$$\overline{\delta^{\zeta_{c1}}} = 0 \qquad \text{at } \Gamma_o \tag{C.3a}$$

$$\overline{\delta^{\zeta_{s1}}} = 0 \qquad \text{at } \Gamma_o \tag{C.3b}$$

$$\vec{u}^0_{c1}\cdot\delta^{\vec{u}_{c1}} + \vec{u}^0_{s1}\cdot\delta^{\vec{u}_{s1}} - \delta^\beta\left\langle C^0\right\rangle - \beta^0\delta^{\langle C\rangle} = 0 \qquad \text{for } (x,y)\in\Gamma_o, \tag{C.3c}$$

$$\overline{\delta^h} = 0 \qquad \text{at } \Gamma_o, \tag{C.3d}$$

$$\left[(1-h^0)\,\delta^{\vec{u}_{c1}} - \delta^h\vec{u}^0_{c1}\right]\cdot\vec{n} = 0 \qquad \text{for } (x,y)\in\Gamma_c, \tag{C.3e}$$

$$\left[(1-h^0)\,\delta^{\vec{u}_{s1}} - \delta^h\vec{u}^0_{s1}\right]\cdot\vec{n} = 0 \qquad \text{for } (x,y)\in\Gamma_c, \tag{C.3f}$$

$$\begin{aligned}&\left[a\mu\Lambda\left(\delta^\beta\left\langle C^0\right\rangle\vec{\nabla}h^0 + \beta^0\delta^{\langle C\rangle}\vec{\nabla}h^0 + \beta^0\left\langle C^0\right\rangle\vec{\nabla}\delta^h\right)\right.\\ &\quad\left. + a\mu\vec{\nabla}\delta^{\langle C\rangle} + \lambda\vec{\nabla}\delta^h\right]\cdot\vec{n} = 0 \qquad \text{for } (x,y)\in\Gamma_c.\end{aligned} \tag{C.3g}$$

144 In order to apply the Finite Element Method, the equations have to be written in their weighted
145 residual formulation, by multiplying them with a test function and integrating them over the do-
146 main Ω. The following notation is introduced

$$(f_1, f_2)_\Omega = \int_\Omega f_1 \, f_2 \, \mathrm{d}\Omega. \tag{C.4}$$

147 Applying the Gauss theorem and the boundary conditions (C.3), the weak formulation yields:

$$\begin{aligned}
&\left(\delta^{\zeta_{s1}}, w^{\zeta_{c1}}\right)_\Omega - \left((1-h^0)\,\delta^{\vec{u}_{c1}} - \delta^h\,\vec{u}^0_{c1}, \vec{\nabla} w^{\zeta_{c1}}\right)_\Omega \\
&\quad = \left(-\zeta^0_{s1}, w^{\zeta_{c1}}\right)_\Omega + \left((1-h^0)\,\vec{u}^0_{c1}, \vec{\nabla} w^{\zeta_{c1}}\right)_\Omega,
\end{aligned} \tag{C.5a}$$

$$\begin{aligned}
&\left(-\delta^{\zeta_{c1}}, w^{\zeta_{s1}}\right)_\Omega - \left((1-h^0)\,\delta^{\vec{u}_{s1}} - \delta^h\,\vec{u}^0_{s1}, \vec{\nabla} w^{\zeta_{s1}}\right)_\Omega \\
&\quad = \left(\zeta^0_{c1}, w^{\zeta_{s1}}\right)_\Omega + \left((1-h^0)\,\vec{u}^0_{s1}, \vec{\nabla} w^{\zeta_{s1}}\right)_\Omega,
\end{aligned} \tag{C.5b}$$

$$\begin{aligned}
&\left((1-h^0+h_0)\left[\delta^{\vec{u}_{s1}} + \eta^{-2}\vec{\nabla}\delta^{\zeta_{c1}} + \mathbf{F}\cdot\delta^{\vec{u}_{c1}}\right], w^{\vec{u}_{c1}}\right)_\Omega \\
&\quad - \left(\delta^h\left[\vec{u}^0_{s1} + \eta^{-2}\vec{\nabla}\zeta^0_{c1} + \mathbf{F}\cdot\vec{u}^0_{c1}\right], w^{\vec{u}_{c1}}\right)_\Omega + \left(r\delta^{\vec{u}_{c1}}, w^{\vec{u}_{c1}}\right)_\Omega \\
&\quad = -\left((1-h^0+h_0)\left[\vec{u}^0_{s1} + \eta^{-2}\vec{\nabla}\zeta^0_{c1} + \mathbf{F}\cdot\vec{u}^0_{c1}\right], w^{\vec{u}_{c1}}\right)_\Omega - \left(r\vec{u}^0_{c1}, w^{\vec{u}_{c1}}\right)_\Omega,
\end{aligned} \tag{C.5c}$$

$$\begin{aligned}
&\left((1-h^0+h_0)\left[-\delta^{\vec{u}_{c1}} + \eta^{-2}\vec{\nabla}\delta^{\zeta_{s1}} + \mathbf{F}\cdot\delta^{\vec{u}_{s1}}\right], w^{\vec{u}_{s1}}\right)_\Omega \\
&\quad - \left(\delta^h\left[-\vec{u}^0_{c1} + \eta^{-2}\vec{\nabla}\zeta^0_{s1} + \mathbf{F}\cdot\vec{u}^0_{s1}\right], w^{\vec{u}_{s1}}\right)_\Omega + \left(r\delta^{\vec{u}_{s1}}, w^{\vec{u}_{s1}}\right)_\Omega \\
&\quad = -\left((1-h^0+h_0)\left[-\vec{u}^0_{c1} + \eta^{-2}\vec{\nabla}\zeta^0_{s1} + \mathbf{F}\cdot\vec{u}^0_{s1}\right], w^{\vec{u}_{s1}}\right)_\Omega - \left(r\vec{u}^0_{s1}, w^{\vec{u}_{s1}}\right)_\Omega,
\end{aligned} \tag{C.5d}$$

$$\begin{aligned}
&\left(a\mu\vec{\nabla}\delta^{\langle C\rangle} + a\mu\Lambda\left[\delta^\beta\left\langle C^0\right\rangle\vec{\nabla}h^0 + \beta^0\delta^{\langle C\rangle}\vec{\nabla}h^0 + \beta^0\left\langle C^0\right\rangle\vec{\nabla}\delta^h\right], \vec{\nabla} w^{\langle C\rangle}\right)_\Omega \\
&\quad + \left(\lambda\vec{\nabla}\delta^h\cdot\vec{n}, w^{\langle C\rangle}\right)_{\Gamma_c} - \left(\vec{u}^0_{c1}\cdot\delta^{\vec{u}_{c1}} + \vec{u}^0_{s1}\cdot\delta^{\vec{u}_{s1}} - \delta^\beta\left\langle C^0\right\rangle - \beta^0\delta^{\langle C\rangle}, w^{\langle C\rangle}\right)_\Omega \\
&\quad = -\left(a\mu\vec{\nabla}\left\langle C^0\right\rangle + a\mu\Lambda\beta^0\left\langle C^0\right\rangle\vec{\nabla}h^0, \vec{\nabla} w^{\langle C\rangle}\right)_\Omega - \left(\lambda\vec{\nabla}h^0\cdot\vec{n}, w^{\langle C\rangle}\right)_{\Gamma_c} \\
&\quad + \left(\frac{1}{2}|\vec{u}^0_{c1}|^2 + \frac{1}{2}|\vec{u}^0_{s1}|^2 - \beta^0\left\langle C^0\right\rangle, w^{\langle C\rangle}\right)_\Omega,
\end{aligned} \tag{C.5e}$$

$$\begin{aligned}
&\left(a\mu\vec{\nabla}\delta^{\langle C\rangle} + a\mu\Lambda\left[\delta^\beta\left\langle C^0\right\rangle\vec{\nabla}h^0 + \beta^0\delta^{\langle C\rangle}\vec{\nabla}h^0 + \beta^0\left\langle C^0\right\rangle\vec{\nabla}\delta^h\right] + \lambda\vec{\nabla}\delta^h, \vec{\nabla} w^h\right)_\Omega \\
&\quad = -\left(a\mu\vec{\nabla}\left\langle C^0\right\rangle + a\mu\Lambda\beta^0\left\langle C^0\right\rangle\vec{\nabla}h^0 + \lambda\vec{\nabla}h^0, \vec{\nabla} w^h\right)_\Omega,
\end{aligned} \tag{C.5f}$$

with the Dirichlet boundary conditions

$$\overline{\delta^{\zeta_{c1}}} = 0 \qquad \text{at } \Gamma_o \tag{C.6a}$$

$$\overline{\delta^{\zeta_{s1}}} = 0 \qquad \text{at } \Gamma_o \tag{C.6b}$$

$$\vec{u}^0_{c1}\cdot\delta^{\vec{u}_{c1}} + \vec{u}^0_{s1}\cdot\delta^{\vec{u}_{s1}} - \delta^\beta\left\langle C^0\right\rangle - \beta^0\delta^{\langle C\rangle} = 0 \qquad \text{for } (x,y)\in\Gamma_o. \tag{C.6c}$$

Appendix D Analysis of the width-averaged morphodynamic equilibria for exponentially converging and diverging basins by analytical approximations

To explain the findings with respect to the longitudinal structure of the 2DH morphodynamic equilibria of section 3.1 in the main text, the focus of this section is on morphodynamic equilibria in a 1DH-model formulation. We start with an analytical approximation for an equilibrium bed profile in a rectangular tidal basin. Afterwards, tidal basins with width variation are considered as well.

In the width-averaged model, considering the boundary condition (2.7b), the bed evolution equation (2.9) reduces to

$$\langle q^x \rangle = 0 \Leftrightarrow \left\langle -\rho_s (1-p)\lambda h_x - \mu C_x - \mu \frac{w_s}{\kappa_v} \beta C h_x \right\rangle = 0. \tag{D.1}$$

where $\langle q^x \rangle$ denotes the total tidally- and width-averaged sediment transport rate, i.e. the longitudinal component of $\langle q \rangle$. Assuming an approximate balance between erosion and deposition, it can be deduced from equation (2.3) that

$$\langle C \rangle = \frac{\alpha \kappa_v}{w_s^2} \frac{\langle u^2 \rangle}{\beta}. \tag{D.2}$$

Neglecting the bed load transport and using equation (2.4), the equation (D.1) can be rewritten as

$$\langle q^x \rangle = \mu \frac{\alpha \kappa_v}{w_s^2} \left[\left(\frac{\langle u^2 \rangle}{\beta} \right)_x + \frac{w_s}{\kappa_v} \beta \frac{\langle u^2 \rangle}{\beta} h_x \right] = 0 \tag{D.3a}$$

$$\Leftrightarrow \frac{\langle 2u\, u_x \rangle}{\beta} - \langle u^2 \rangle \frac{\beta_x}{\beta^2} + \frac{w_s}{\kappa_v} \langle u^2 \rangle h_x = 0 \tag{D.3b}$$

To a first approximation, neglecting friction and local inertia, the hydrodynamics can be described by a so-called pumping mode, where the momentum equation reduces to $\zeta_x = 0$ throughout the channel (Schuttelaars & de Swart, 1996). Given the continuity equation (2.1a) and the boundary condition (2.2a), with $\theta_{M_2} = 0$, the velocity in a rectangular basin can be approximated by

$$u = \left[A_{M_2} \sigma \frac{x - L}{\overline{H} - h} \right] \sin(\sigma t) \tag{D.4}$$

where the expression in between the square brackets is referred to as the spatial coefficient of the time-dependent velocity u hereafter. Thus

$$\langle 2u\, u_x \rangle = A_{M_2}^2 \sigma^2 \frac{(x-L)(\overline{H}-h) + (x-L)^2 h_x}{(\overline{H}-h)^3} = A_{M_2}^2 \sigma^2 (x-L) \frac{(\overline{H}-h) + (x-L) h_x}{(\overline{H}-h)^3}, \tag{D.5}$$

where we used that $\left\langle \sin^2(\sigma t) \right\rangle = \frac{1}{2}$.

Now two distinct cases are considered:

- Diffusively dominated transport with a constant deposition parameter, i.e. the topographically induced transport is neglected and $\beta = 1$.
  In this case, equation (D.2) simplifies to

$$\langle 2u\, u_x \rangle = 0. \tag{D.6}$$

Using equation (D.5) and disregarding the landward boundary ($x = L$) where $h = \overline{H}$, the expression can be written as

$$h_x = \frac{\overline{H} - h}{L - x}, \tag{D.7}$$

which implies a linearly sloping bed profile $h = \frac{\overline{H}}{L}x$, corresponding to the findings of Schuttelaars and de Swart (1996).

- Combined transport with a depth-dependent deposition parameter.
  In this case, by plugging the deposition parameter formulation (2.4) in, the equation (D.3b) can be rewritten as

$$\langle 2u\, u_x \rangle = \left\langle u^2 \right\rangle \frac{w_s}{\kappa_v} \beta h_x \left[e^{-\frac{w_s}{\kappa_v}(\overline{H} - h + h_0)} - 1 \right], \tag{D.8a}$$

$$\Leftrightarrow \langle 2u\, u_x \rangle = -\left\langle u^2 \right\rangle \frac{w_s}{\kappa_v} h_x. \tag{D.8b}$$

Since it is assumed that $h_x > 0$, the right hand side of equation (D.8b) will always be negative, which implies that $\langle 2u\, u_x \rangle < 0$. Since the spatial coefficient of u in equation (D.4) is always negative, it follows that the spatial coefficient of u_x has to be positive, i.e. the velocity magnitude decreases towards the landward end. As in the previous case, it can be deduced that

$$h_x < \frac{\overline{H} - h}{L - x} = \frac{h(L) - h(x)}{L - x}. \tag{D.9}$$

The equality follows from the requirement that the water depth at the landward side vanishes. This indicates that for any $0 \leq x < L$, the local derivative is smaller than the slope of the secant line between x and L. Using the mean value theorem, it follows that the derivative will monotonically increase, which implies that the bed level has a convex shape. This agrees with the findings of Ter Brake and Schuttelaars (2011).

For a tidal basin with an exponentially converging or diverging width, equation (D.4) changes to

$$u = \left[A_{M_2} \sigma L_c \frac{1 - e^{\frac{x-L}{L_c}}}{\overline{H} - h} \right] \sin(\sigma t), \tag{D.10}$$

as was shown in Meerman et al. (2019). In the case of diffusively dominated transport with a constant deposition parameter $\beta = 1$, u is constant throughout the domain and thus

$$h \sim \overline{H} - \frac{A_{M_2} \sigma L_c}{\hat{u}} \left(1 - e^{\frac{x-L}{L_c}} \right). \tag{D.11}$$

with $\hat{u}$ a certain velocity scale. This implies that for a converging tidal basin ($L_c > 0$) the first and second derivatives of the bed level are positive and the morphodynamic equilibrium is convex. For a diverging tidal basin ($L_c < 0$), on the other hand, the first derivative is positive, but the second derivative is negative, resulting in a concave equilibrium bed level.

The behaviour in Fig. 3 can be interpreted as follows. The combination of the diffusive and the topographically induced sediment transport, together with a depth-dependent deposition pa-

rameter, favours a convex equilibrium bed profile. For an exponentially converging inlet, this convexity is enhanced, while for an exponentially diverging tidal basin, the convexity is reduced or even overcome for strongly diverging basins.

Appendix E Influence of the Coriolis force in a rectangular basin

The influence of the Coriolis force is investigated for a rectangular tidal inlet system with a length and width of 15 km. By gradually increasing the Coriolis coefficient f from 0 to $1.0 \cdot 10^{-4}$ rad s^{-1} , a series of 2DH morphodynamic equilibria is obtained. The equilibrium bed corresponding to the largest value of the Coriolis parameter considered, is shown in Fig. E.1a. From this figure is follows that the water depth is not symmetric anymore, and that the equilibrium bed is not laterally uniform at the seaward boundary. Note however, that the width–averaged depth $\overline{h}$ is 0 m at this location, thus satisfying the prescribed boundary condition for h. In Figs E.1b, E.1c, and E.1d the corresponding tidally–averaged concentration and the amplitudes of the longitudinal and transverse velocities are shown, respectively. To clearly visualize the symmetry breaking effect due to the Coriolis force, cross-sectional profiles at different locations in the longitudinal direction are shown in Fig. E.1e. In this figure, solid lines denote the cross–channel bathymetries obtained when Coriolis effects are included. For comparison, the lateral bathymetries obtained when ignoring Coriolis effects are indicated by dashed lines. These dashed lines clearly show that for a rectangular tidal inlet system without Coriolis effects taken into account, the 2DH equilibrium bathymetry has no lateral variations. The inclusion of Coriolis effects results in an equilibrium morphology that has lateral variations and is not symmetric anymore around $y = 0$. To quantify this, the relative position of the cross-sectional centroids y_c/B is shown in Fig. E.1f as a function of the distance to the seaward boundary (horizontal axis) and the Coriolis parameter f (vertical axis), with y_c defined in equation 3.5. The dashed line indicates locations where $y_c/B = 0$. From this figure it follows that in the largest part of the domain, the bed is deeper near the left boundary than near the right boundary (negative y_c/B), due to Coriolis effects. This asymmetry increases with increasing the Coriolis parameter f. Only close to the landward boundary, the water depth becomes larger near the right boundary, compared to the water depth near the left boundary.

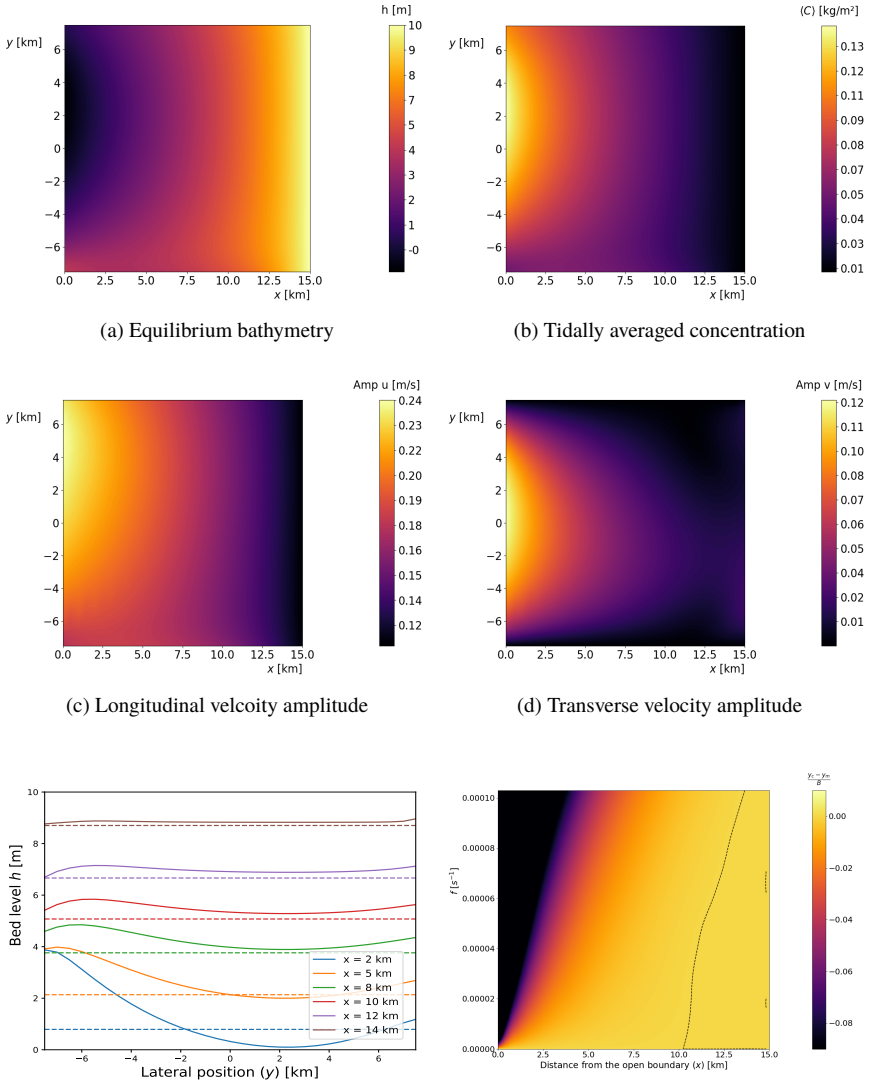

Figure E.1. (a) The 2DH equilibrium bed profile for simulation with the Coriolis effect, for a rectangular basin. (b) The equilibrium concentration profile. (c) The amplitude of the longitudinal velocity (d) The amplitude of the transverse velocity (e) five cross sections of the equilibrium bed level at different distances from the open boundary (f) The relative position of the cross-sectional centroids y_c/B as a function of the longitudinal position (horizontal axis) and the Coriolis parameter f.

Appendix F Asymmetric geometry with a laterally uniform bed

In this appendix, the physical mechanisms resulting in morphodynamic equilibria associated with an asymmetric tidal inlet system are explained. The asymmetry is caused by an asymmetric geometry (see section 3.2.2 of the main text), characterised by a width at the landward boundary $B_l = 20$ km. The corresponding 2DH equilibrium bathymetry is shown in Fig. 7b of the main text. Following the approach discussed in section 4.2, the dynamics associated with a prescribed bathymetry that is laterally uniform is used to explain the resulting channel–shoal pat-

tern. The longitudinal depth variation of the laterally uniform bed is given by the profile obtained by width–averaging the 2DH equilibrium bathymetry.

In Fig. F.2c the amplitude of the longitudinal velocity is shown. Compared to the symmetric case (Fig. 10c in the main text), the amplitude no longer decreases when moving toward the landward side. Again, the smallest longitudinal velocities are found near the sidewalls, where the width variations are most pronounced. The transverse velocity amplitudes (Fig. F.2d) are now highest near the left sidewall, where the basin is most strongly widening. These velocities are twice as large as the maximal longitudinal velocity amplitudes. The areas in the tidal inlet system with the highest velocity amplitude, found near the left boundary near km 11, have the highest suspended sediment concentrations (see Fig. F.2b).

Since the prescribed bed profile is a solution of the width–averaged 2DH equilibrium bathymetry, the divergences and convergences of the longitudinal components of the topographically induced and the diffusive transports approximately balance each other (see Figs. F.2e and F.2f). The transport component resulting from lateral gradients in the depth–integrated concentration fields is not balanced at all, resulting in a residual transport of sediments away from the region with high concentration, towards locations with a much smaller suspended sediment concentration, found close to the central axis of the tidal inlet system. This results in a deepening near the sidewalls and accretion close to the central axis, resulting in the formation of a shoal. Since the suspended sediment concentration is asymmetric, this results in more deposition closer to the right boundary, and a smaller and more shallow channel close to the right boundary, compared to the channel on the left (see Fig. 7b for the resulting channel–shoal pattern). By the presence of lateral gradients in the bathymetry, the lateral diffusive transport associated with these gradients (i.e., the lateral component of the topographically induced transport) will be non–zero and approximately balance the lateral sediment transport related to lateral gradients in the depth–integrated suspended sediment concentration.

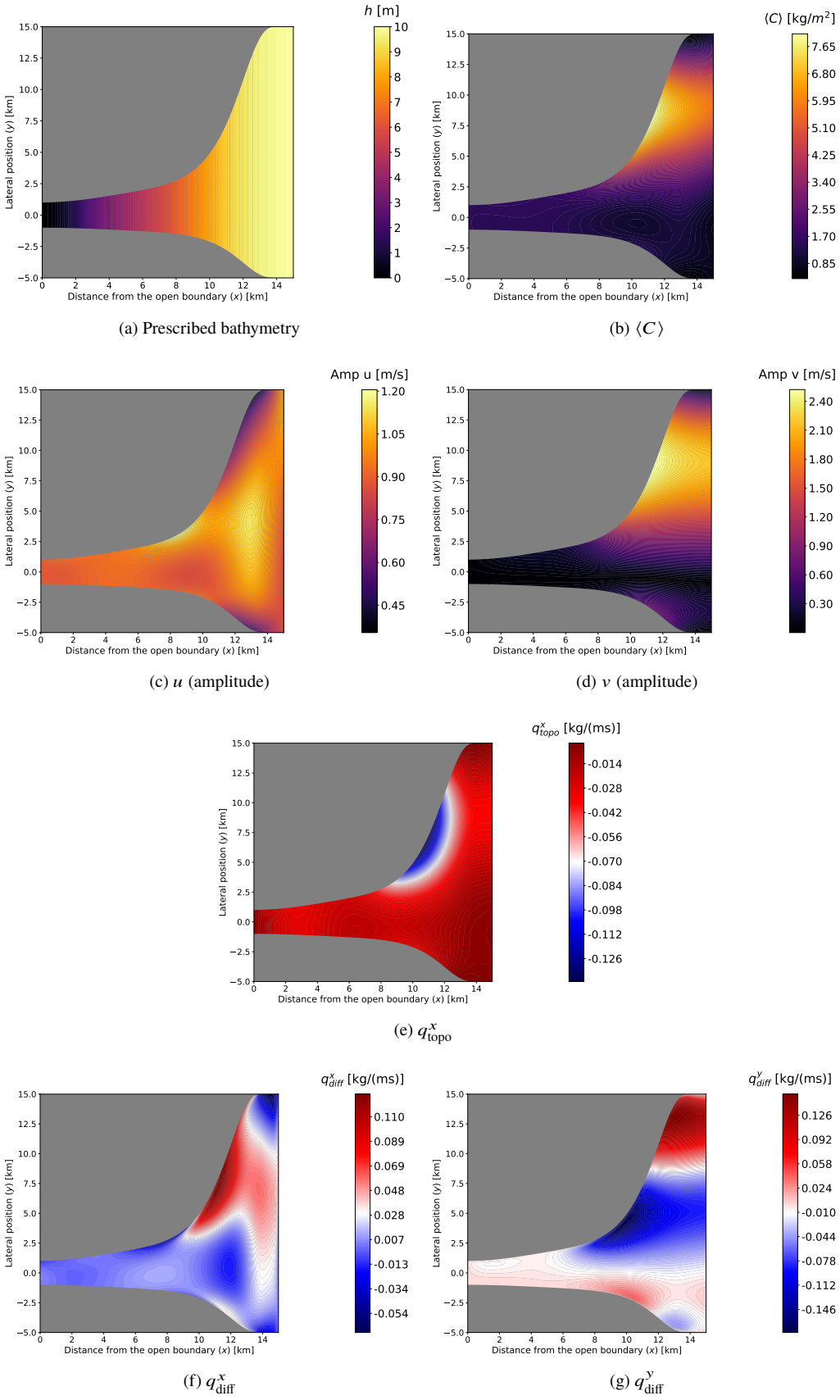

(a) Prescribed bathymetry

(b) $\langle C \rangle$

(c) u (amplitude)

(d) v (amplitude)

(e) q^x_{topo}

(f) q^x_{diff}

(g) q^y_{diff}

Figure F.2. Two-dimensional results of a simulation with a fixed and laterally uniform bed, based on the cross-sectionally averaged morphodynamic equilibrium. (a) the laterally unifrom prescribed bathymetry (b) the tidally averaged suspended sediment concentration (c) the amplitude of the longitudinal velocity, (d) the amplitude of the transverse velocity, (e) the longitudinal component of the topographically induced sediment transport, (f) the longitudinal component of the diffusive sediment transport,(g) the lateral component of the diffusive sediment transport.

References

de Swart, H. E., & Blaas, M. (1998). Morphological evolutions in a 1D model for a dissipative tidal embayment. In J. J. Dronkers & M. B. Scheffers (Eds.), *Physics of Estuaries and Coastal Sea* (pp. 305–314). Rotterdam, The Netherlands: Balkema.

De Vriend, H., & Ribberink, J. (1996). Mathematical modelling of meso-tidal barrier island coasts. Part II: Process-based simulation models. In P. L. Liu (Ed.), *Advances in Coastal and Ocean Engineering* (p. 151-197). Singapore.

Meerman, C., Rottschäfer, V., & Schuttelaars, H. M. (2019). Influence of geometrical variations on morphodynamic equilibria in short tidal basins. *Ocean Dynamics*, *69*(2), 221–238.

Schuttelaars, H. M., & de Swart, H. E. (1996). An idealized long-term morphodynamic model of a tidal embayment. *European Journal of Mechanics B Fluids*, *15*, 55–80.

Ter Brake, M. C., & Schuttelaars, H. M. (2010). Modeling equilibrium bed profiles of short tidal embayments. *Ocean Dynamics*, *60*(2), 183–204.

Ter Brake, M. C., & Schuttelaars, H. M. (2011). Channel and shoal development in a short tidal embayment: an idealized model study. *Journal of Fluid Mechanics*, *677*, 503–529.

van Leeuwen, S. M. (2002). *Tidal inlet systems: bottom pattern formation and outer delta development* (PhD thesis). Utrecht University, Utrecht, The Netherlands.

van Leeuwen, S. M., & de Swart, H. E. (2001). The effect of advective processes on the morphodynamic stability of short tidal embayments. *Physics and Chemistry of the Earth, Part B: Hydrology, Oceans and Atmosphere*, *26*(9), 735–740.

van Leeuwen, S. M., & de Swart, H. E. (2004). Effect of advective and diffusive sediment transport on the formation of local and global bottom patterns in tidal embayments. *Ocean Dynamics*, *54*(3-4), 441–451.